MVA-CoV2-S vaccine candidate confers full protection from SARS-CoV-2 brain infection and damage in susceptible transgenic mice

Javier Villadiego (fvilladiego@us.es)
Instituto de Biomedicina de Sevilla (IBiS), Hospital Universitario Virgen del Rocío/CSIC/Universidad de Sevilla https://orcid.org/0000-0003-2131-9013

Juan García-Arriaza
Centro Nacional de Biotecnología (CNB), Consejo Superior de Investigaciones Científicas (CSIC)

Reposo Ramírez-Lorca
Instituto de Biomedicina de Sevilla (IBiS), Hospital Universitario Virgen del Rocío/CSIC/Universidad de Sevilla

Daniel Cabello-Rivera
Instituto de Biomedicina de Sevilla (IBiS), Hospital Universitario Virgen del Rocío/CSIC/Universidad de Sevilla

María I. Álvarez-Vergara
Instituto de Biomedicina de Sevilla (IBiS), Hospital Universitario Virgen del Rocío/CSIC/Universidad de Sevilla

Fernando Cala-Fernández
Instituto de Biomedicina de Sevilla (IBiS), Hospital Universitario Virgen del Rocío/CSIC/Universidad de Sevilla

Roberto García-Swinburn
Instituto de Biomedicina de Sevilla (IBiS), Hospital Universitario Virgen del Rocío/CSIC/Universidad de Sevilla https://orcid.org/0000-0002-8154-0265

Ernesto García-Roldán
Instituto de Biomedicina de Sevilla (IBiS), Hospital Universitario Virgen del Rocío/CSIC/Universidad de Sevilla

Juan L. López-Ogáyar
Instituto de Biomedicina de Sevilla (IBiS), Hospital Universitario Virgen del Rocío/CSIC/Universidad de Sevilla

Carmen Zamora
Centro Nacional de Biotecnología (CNB), Consejo Superior de Investigaciones Científicas (CSIC)

David Astorgano
Centro Nacional de Biotecnología (CNB), Consejo Superior de Investigaciones Científicas (CSIC)

Patricia Pérez

Centro Nacional de Biotecnología (CNB), Consejo Superior de Investigaciones Científicas (CSIC)

Alicia Rosales-Nieves

Instituto de Biomedicina de Sevilla (IBiS), Hospital Universitario Virgen del Rocio/CSIC/Universidad de Sevilla. 41013 Seville https://orcid.org/0000-0001-9119-1604

Ana M. Muñoz-Cabello

Instituto de Biomedicina de Sevilla (IBiS), Hospital Universitario Virgen del Rocío/CSIC/Universidad de Sevilla https://orcid.org/0000-0002-8047-768X

Alberto Pascual

hospital universitario virgen del rocio/CSIC/Universidad de Sevilla https://orcid.org/0000-0001-5459-6207

Mariano Esteban

Centro Nacional de Biotecnología (CNB), Consejo Superior de Investigaciones Científicas (CSIC)

Jose Lopez-Barneo

University of Seville

Juan Toledo-Aral

University of Seville

Article

Keywords: SARS-CoV-2, COVID-19, brain infection, neurodegeneration, vaccine MVA-CoV2-S efficacy, transgenic K18-hACE2 mice

Posted Date: February 4th, 2022

DOI: https://doi.org/10.21203/rs.3.rs-1324885/v1

MVA-CoV2-S vaccine candidate confers full protection from SARS-CoV-2 brain infection and damage in susceptible transgenic mice

Javier Villadiego[1,2,3,†,*], Juan García-Arriaza[4,5,†,*], Reposo Ramírez-Lorca[1,2], Daniel Cabello-Rivera[1,2,3], María I. Álvarez-Vergara[1], Fernando Cala-Fernández[1], Roberto García-Swinburn[1,2], Ernesto García-Roldán[1], Juan L. López-Ogáyar[1], Carmen Zamora[4], David Astorgano[4], Patricia Pérez[4,5], Alicia E. Rosales-Nieves[1,3], Ana M. Muñoz-Cabello[1,2,3], Alberto Pascual[1,3], Mariano Esteban[4], José López-Barneo[1,2,3] and Juan José Toledo-Aral[1,2,3,*]

[1] Instituto de Biomedicina de Sevilla (IBiS), Hospital Universitario Virgen del Rocío/CSIC/Universidad de Sevilla, Sevilla, Spain.

[2] Departamento de Fisiología Médica y Biofísica, Facultad de Medicina, Universidad de Sevilla, Sevilla, Spain.

[3] Centro de Investigación Biomédica en Red sobre Enfermedades Neurodegenerativas (CIBERNED), Madrid, Spain

[4] Departamento de Biología Molecular y Celular, Centro Nacional de Biotecnología (CNB), Consejo Superior de Investigaciones Científicas (CSIC), Madrid, Spain.

[5] Centro de Investigación Biomédica en Red de Enfermedades Infecciosas (CIBERINFEC), Madrid, Spain.

† These authors have contributed equally to this work and share first authorship

* Correspondence: fvilladiego@us.es (J.V.); jfgarcia@cnb.csic.es (J.G.-A.); juanjo@us.es (J.J.T.-A.)

Running tittle: MVA-CoV2-S vaccine protects the brain from SARS-CoV-2 infection

Keywords: SARS-CoV-2, COVID-19, brain infection, neurodegeneration, vaccine MVA-CoV2-S efficacy, transgenic K18-hACE2 mice

Abstract

The protective efficacy of vaccines against SARS-CoV-2 infection in the brain is yet unclear. Here, in the susceptible transgenic K18-hACE2 mouse model of severe COVID-19 disease, we report a detailed spatiotemporal description of the SARS-CoV-2 infection and replication in different areas of the brain. Remarkably, SARS-CoV-2 brain replication occurs primarily in neurons, producing important neuropathological alterations such as neuronal loss, incipient signs of neuroinflammation, and vascular damage in SARS-CoV-2 infected mice. Notably, one or two doses of a modified vaccinia virus Ankara (MVA) vector expressing the SARS-CoV-2 spike (S) protein (MVA-CoV2-S) conferred full protection against SARS-CoV-2 cerebral infection, preventing virus replication in all areas of the brain and its associated damage. This protection was maintained even after SARS-CoV-2 reinfection. To our knowledge, this is the first study of a COVID-19 vaccine candidate showing 100% efficacy against SARS-CoV-2 brain infection and damage, reinforcing the use of MVA-CoV2-S as a promising vaccine candidate against SARS-CoV-2/COVID-19, worth to move forward into clinical trials.

Introduction

Coronavirus disease 2019 (COVID-19) is caused by the infection of the severe acute respiratory syndrome coronavirus 2 (SARS-CoV-2)[1]. Although COVID-19 is primarily a respiratory disease, many patients manifest neurological symptoms, including anosmia and ageusia, nonspecific symptoms such as headache or dizziness, or severe conditions such as cognitive impairment, epilepsy, ataxia, or encephalopathy[2]. These symptoms have been attributed to either secondary effects of the systemic alterations (i.e. produced by the hypoxemia, plasma electrolyte dysregulation or cytokine storm) or the direct infection of the central nervous system (CNS) by SARS-CoV-2[3–6]. Direct CNS infection is supported by the neurotropism exhibited by other coronaviruses[7–9] and by the detection of SARS-CoV-2 in cerebrospinal fluid from COVID-19 patients and in a significant proportion of brain autopsies from patients who died from COVID-19[3,10,11]. Furthermore, SARS-CoV-2 has also been detected in the brain of different experimental animal models, including transgenic[12,13] and knock-in mice[14] expressing human angiotensin-converting enzyme 2 (hACE2) as well as natural hosts of SARS-CoV-2 such as hamsters[6,15], ferrets[16] and non-human primates[17,18]. Regardless of the pathogenic mechanism (viral neuroinvasion or secondary to the systemic infection) several studies have demonstrated important neuropathological alterations in severe COVID-19 patients, such as neurovascular pathology, neuroinflammation, and neuronal damage[11,19–21]. Additionally, biomarkers of cerebral injury have also been found to be elevated in patients with mild or moderate COVID-19[22,23]. Furthermore, neurological manifestations are common in patients recovered from the acute phase of COVID-19, suggesting the possibility of chronic brain impairment associated to the post-acute COVID-19 syndrome[24–26].

Numerous vaccine candidates against COVID-19 have been developed and clinically tested in phase I/II/III trials. Vaccines approved by the main regulatory agencies (FDA in USA or EMA in Europe) are primarily based on the SARS-CoV-2 spike (S) protein and have been generated by different technologies including mRNA (Pfizer/BioNTech and Moderna)[27,28], adenoviral vectors (AstraZeneca, Janssen and Sputnik)[29–31] or inactivated virus (Sinopharm and Sinovac)[32]. Although these vaccines have shown remarkable efficacy against the severe effects of the disease, they do not confer sterilizing immunity as viral replication has been detected in the respiratory tract of vaccinated individuals[33,34]. These vaccines are currently being used for mass vaccination; however, it is still unknown whether they prevent viral spread to other regions of the body such as the CNS and confer protection against the brain damage induced by the SARS-CoV-2 infection.

We have previously described the advantages of a poxvirus modified vaccinia virus Ankara (MVA) vector expressing a human codon optimized full-length SARS-CoV-2 S protein (termed MVA-CoV2-S) as a promising COVID-19 vaccine candidate. MVA-CoV2-S vaccine candidate induces in mice robust and long-term memory S-specific humoral and T cellular immune responses, and fully prevented morbidity, mortality, and viral replication and pathology in the lungs of K18-hACE2 transgenic mice[35–37]. Here, we examine the efficacy of MVA-CoV2-S vaccination to prevent SARS-CoV-2 cerebral infection and associated damage in K18-hACE2 mice, a well-established mouse model of severe COVID-19 disease[12,13,38]. To this end, we provide a detailed spatiotemporal description of the SARS-CoV-2 viral spread among the main regions of the brain. Interestingly, SARS-CoV-2 infection and replication appear mainly restricted to neurons, producing a significant neuronal cell death. Indeed, as previously described[20], infected

mice also exhibit pathological alterations in brain blood vessels. Importantly, administration of one or two doses of the MVA-CoV2-S vaccine candidate confers full protection against SARS-CoV-2 neuroinvasion, preventing cerebral viral replication and the associated brain damage, even after reinfection. To our knowledge, this is the first study of a COVID-19 vaccine showing 100% efficacy against SARS-CoV-2 brain infection and damage, postulating MVA-CoV2-S as a promising vaccine candidate against SARS-CoV-2/COVID-19, worth to move forward into clinical trials.

Results

Characterization of SARS-CoV-2 brain infection in K18-hACE2 transgenic mice.

Although SARS-CoV-2 CNS neurotropism has previously been described[3,4,13], little information about viral spreading to specific cerebral areas has been reported. Thus, to study in detail the spatiotemporal SARS-CoV-2 viral distribution and replication in the brain, K18-hACE2 mice (n=11) were intranasally inoculated with SARS-CoV-2 [MAD6 isolate, 1 x 10^5 plaque-forming units (PFU)/mouse][35,36] and their brains were examined by immunohistochemistry against SARS-CoV-2 nucleocapsid (N) protein at 2 (n=3), 4 (n=3) and 6 (n=5) days post infection (dpi) (Fig. 1 and Supplementary Fig. 1). At 6 dpi all mice infected with SARS-CoV-2 lost more than 25% of body weight and were sacrificed[35,36]. Figure 1A shows brain coronal sections from representative control (uninfected) and SARS-CoV-2-infected mice (6 dpi) revealing that the SARS-CoV-2 N staining was clear and specific, with numerous infected cells throughout different regions of the brain. The precise analysis of the brain viral distribution at different time points is depicted in Figures 1B,C and Supplementary Figure 1. At 2 dpi, no evidence of SARS-CoV-2 infection was found in any of the brain areas studied in the 3 mice analyzed.

At 4 dpi, variable levels of viral infection were observed in the different cerebral regions examined in the 3 mice analized. Specifically, the basal forebrain, the amygdala, and the hypothalamus showed the highest levels of viral infection at this time point, with numerous groups of SARS-CoV-2 infected cells in most of the brains analyzed. In other regions such as the olfactory bulb, cortex or mesencephalon, an intermediate level of infection was detected, with only some dispersed infected cells in most of the brains studied. In contrast, in other cerebral regions like the striatum, hippocampus, thalamus, pons and cerebellum, only 1 of the 3 brains analyzed showed some few SARS-CoV-2^{+} cells, indicating the lower level of infection at 4 dpi. Finally, at the latest time point studied, 6 dpi, all brains analyzed (n=5) revealed high levels of SARS-CoV-2 N staining, but showed a non-homogeneous distribution of viral infection among the main areas of the brain. In the olfactory bulbs, cortex, basal forebrain, amygdala, thalamus, hypothalamus and mesencephalon, a severe SARS-CoV-2 infection was detected. Other regions such as the hippocampus and pons showed moderate infection, whereas in the striatum and cerebellum only some disperse SARS-CoV-2^{+} cells were detected suggesting a mild viral infection.

An important observation revealed by the histological analysis described above is that most of the SARS-CoV-2 infected cells show a neuronal morphology (Fig. 1C and Supplementary Fig. 1), suggesting that viral replication in the brain occurs primarily in neurons. This was confirmed by high resolution confocal microscopy analysis combining SARS-CoV-2 N protein immunofluorescence with neuronal (neuronal-specific nuclear antigen A60; NeuN), astroglial (glial fibrillary acid protein; GFAP), microglial (ionized calcium-binding adapter molecule 1; IBA1) and vascular endothelial (isolectin B4; IB4) markers in SARS-CoV-2 infected brains at 6 dpi. As indicated in Figure 2, all cells showing

high SARS-CoV-2 staining (green) were also positive for the neuronal marker NeuN (red). In addition, a confocal orthogonal projection confirmed that both SARS-CoV-2$^+$ and NeuN$^+$ signals colocalized in the same confocal plane (Z-depth resolution of confocal plane: 0.7 μm; Fig. 2B), indicating that the SARS-CoV-2 N protein and the NeuN protein are within the same neuronal body. On the contrary, the confocal microscopy analysis combining SARS-CoV-2 N protein with astroglial GFAP (Supplementary Fig. 2A), microglial IBA1 (Supplementary Fig. 2B) or vascular IB4 (Supplementary Fig. 2C) proteins revealed the absence of significant SARS-CoV-2 staining in astrocytes, microglia and brain blood vessels, respectively.

Taken together, the histological analysis indicates that SARS-CoV-2 brain replication in K18-hACE2 mice occurs primarily in neurons. This cerebral replication begins between 2-4 days after inoculation with SARS-CoV-2 and occurs at the highest rates in ventral areas of the brain such as the hypothalamus, amygdala, and the basal forebrain. In a later phase, between 4-6 dpi, viral replication spreads to most cerebral regions, producing a severe SARS-CoV-2 infection. Interestingly, even at 6 dpi some specific cerebral areas, such as the cerebellum and striatum, remain with mild levels of SARS-CoV-2 infection, presenting only some dispersed SARS-CoV-2 infected neurons.

Neuropathological alterations associated to SARS-CoV-2 brain infection.

Next, we studied whether the strong SARS-CoV-2 infection induces neuronal death by analyzing the neuronal density in the hypothalamus and cortex, two of the brain areas that display high viral replication. The stereological quantification of hypothalamic NeuN$^+$ (Fig. 3A,B) and cortical Nissl$^+$ (Fig. 3C,D) neurons demonstrated a significant decrease of the neuronal density in SARS-CoV-2-infected mice at 6 dpi,

compared to uninfected mice controls. Since SARS-CoV-2 infection can induce neuronal apoptosis in human brain organoids[5], we studied by immunodetection the number of cells expressing cleaved caspase-3 (c-casp3) in brains from control (uninfected) and SARS-CoV-2-infected mice at 4 and 6 dpi. As expected, the brains of control mice showed only few c-casp3$^+$ cells in the hippocampus (Fig. 3E,F), possibly reflecting physiological apoptosis associated with the neurogenic niche of the dentate gyrus[39], and no c-casp3$^+$ cells were detected in the rest of the brain (Fig. 3G,H and Supp. Fig. 3A,B). In contrast, brains of SARS-CoV-2-infected mice presented a significant number of c-casp3$^+$ cells distributed across most of the brain areas analyzed, being particularly evident at 6 dpi (Fig. 3E-H and Supp. Fig. 3A,B), when the brain viral infection is maximal. The distribution of c-casp3$^+$ cells suggests that a significant proportion of apoptotic cells correspond to neurons. Quantitative analyses of apoptotic cell numbers were performed in the hippocampus (Fig. 3F) and the hypothalamus (Fig. 3H). In both regions, we found a clear trend towards a higher number of c-casp3$^+$ cells in SARS-CoV-2-infected mice, although statistical significance was observed only in the hypothalamus at 6 dpi (Fig. 3H), one of the regions with the highest levels of viral infection (see Fig. 1C).

Neuroinflammation and structural alterations in cerebral blood vessels have been described in COVID-19 patients[20,21]. Thus, to study the neuroinflammatory reaction in brains from K18-hACE2 mice infected with SARS-CoV-2, we analyzed the presence of astrogliosis and reactive microglia using specific immunostaining of astroglial (GFAP) and microglial (IBA1) markers. At 2, 4 and 6 dpi, no signs of astrogliosis were detected, either by GFAP overexpression or by morphological changes in GFAP$^+$ astrocytes, in any of the cerebral regions studied (cortex, hippocampus and hypothalamus) (Supp. Fig. 4A). However, at 6 dpi an increase in IBA1 expression was

observed in the same brain regions, suggesting microglial activation (Supp. Fig. 4A). Given that microglial activation is characterized by an enlargement of the cell body, we carried out a quantitative analysis of the microglial cell body in the cortex of control and SARS-CoV-2-infected mice. Results showed a non-significant trend towards larger cell bodies in infected mice with respect to controls (Supp. Fig. 4B). As animals were sacrificed at 6 dpi (due to a marked loss of body weight) it is likely that the microglial response induced by SARS-CoV-2 infection was still at an early stage. To study the presence of vascular pathology brain blood vessels were labelled with IB4 and vessel abnormality evaluated as previously described[40]. No significant alterations in the cerebral blood vessels of SARS-CoV2 infected mice were found at 2 and 4 dpi. However, at 6 dpi, when brain viral infection is maximal, histological evidence of abnormal blood vessels started to appear in ventral brain areas of infected mice (basal forebrain, amygdala and hypothalamus; Supp. Fig. 4A,C). These results agree with the vascular brain pathology described in COVID-19 patients, hamsters, and K18-hACE2 mice infected with SARS-CoV-2[20]. They also indicate that SARS-CoV-2 infection in the K18-hACE2 mouse model of severe COVID-19 produces important neuropathological alterations, including neuronal loss, incipient signs of neuroinflammation, and vascular damage.

MVA-CoV2-S vaccination fully prevents SARS-CoV-2 brain infection and associated damage.

Once the temporal and regional spread of SARS-CoV-2 and the associated neuropathology were characterized in the brain of K18-hACE2 mice, we next tested whether the vaccine candidate MVA-CoV2-S (also termed MVA-S), expressing the SARS-

CoV-2 S protein[35], could protect against SARS-CoV-2 brain infection and associated damage. Thus, K18-hACE2 mice were immunized by intramuscular (i.m.) route with one or two doses of MVA-S (1 x 10^7 PFU/mouse) at days 0 and 28, and subsequently, on day 63, challenged with a lethal intranasal (i.n.) dose of SARS-CoV-2 (MAD6 isolate; 1 x 10^5 PFU/mouse), as we have previously reported[35,36]. SARS-CoV-2 challenged mice primed and boosted with MVA-WT (wild-type empty MVA vector) were used as control (Fig. 4A, upper panels). Then at 4 dpi (day 67) 3 mice per group were sacrificed for brain extraction and processing. Moreover, in a second independent experimental approach, we evaluated whether mice vaccinated with one or two doses of MVA-S, which survived to SARS-CoV-2 infection[35], were protected against viral neuroinvasion following a SARS-CoV-2 reinfection performed 46 days after the first SARS-CoV-2 challenge. In this experiment, challenged unvaccinated and MVA-WT inoculated mice were used as controls (Fig. 4A, lower panels). Thereafter, mice (n=5 per group) were sacrificed for brain extraction and processing 6 days after the second viral infection (6 dpi) or at 6 days after the first infection in the unvaccinated and MVA-WT groups. In both experimental approaches, the presence of cerebral SARS-CoV-2 infection was analyzed by immunohistochemistry against the SARS-CoV-2 N protein in different brain regions, as described above. Interestingly, all MVA-S vaccinated mice, either with one or two doses, showed total protection against cerebral SARS-CoV-2 infection after a single SARS-CoV-2 infection (Fig. 4B,C) or after a reinfection (Fig. 4C and Supplementary Fig. 5), without any SARS-CoV-2^+ infected cell being detected in any of the brain regions analyzed. The absence of SARS-CoV-2^+ immunostaining observed in MVA-S vaccinated mice contrast with the high number of SARS-CoV-2^+ infected cells found in challenged MVA-WT inoculated mice (Fig. 4B,C and Supplementary Fig. 5) or in challenged unvaccinated mice

(Fig. 4C and Supplementary Fig. 5). Furthermore, to discard the possibility that the absence of SARS-CoV-2$^+$ labeling in MVA-S vaccinated mice was due to a low viral load, which could be below the immunohistochemistry detection limit, we performed highly sensitive real-time RT-PCR of the SARS-CoV-2 E gene in the cortex and hypothalamus, two brain regions that present high viral replication. According to the histological analysis, SARS-CoV-2 subgenomic mRNA was not detected in mice vaccinated with one or two doses of MVA-S, neither after a single SARS-CoV-2 infection (Fig. 4D) nor after reinfection (Fig. 4E). In contrast, high levels of SARS-CoV-2 subgenomic mRNA were found in the cortex and hypothalamus of SARS-CoV-2 challenged MVA-WT or unvaccinated mice. These results demonstrate that MVA-S confers complete and sustained protection against SARS-CoV-2 cerebral infection.

We also evaluated the efficacy of MVA-S vaccination to protect against brain damage induced by severe SARS-CoV-2 infection. Stereological quantification of the density of hypothalamic NeuN$^+$ (Fig. 5A) and cortical Nissl$^+$ (Fig. 5B) neurons clearly demonstrated that MVA-S vaccination, either with one or two doses, protects against the neurodegeneration induced by SARS-CoV-2 infection. Furthermore, analysis of apoptotic cells revealed the absence of c-casp3$^+$ cells in all brains of MVA-S vaccinated mice, with the exception of physiological hippocampal apoptosis also detected in uninfected mice (data not shown). Quantification of the number of c-casp3$^+$ cells in the hypothalamus confirmed that MVA-S vaccination confers a complete protection against CNS cellular apoptosis induced by SARS-CoV-2 infection (Fig. 5C). Similarly, the analysis of brain blood vessels, after IB4 immunostaining, also showed protection in MVA-S vaccinated mice against the appearance of abnormal brain blood vessels after SARS-CoV-2 infection (Fig. 5D,E). Moreover, the qualitative analysis of microglial IBA1$^+$ cells

indicated lower levels of IBA1 expression in MVA-S vaccinated mice relative to SARS-CoV-2 infected mice, showing a similar pattern of microglial IBA1^{+} staining to uninfected controls (Fig. 5D,F).

Taken together, these data demonstrate that MVA-S vaccination confers a complete protection against SARS-CoV-2 brain infection and the associated neuropathological damage (neuronal loss, neuroinflammation, and vascular damage), even after a second viral infection. Interestingly, cerebral protection induced by MVA-S vaccine candidate is achieved similarly with one or two doses.

Discussion

After respiratory symptoms, neuropsychiatric manifestations are the second most common symptoms in COVID-19 patients, with a wide range of signs that differ in their severity and time at which they occur[2,24,41]. Despite the clinical relevance of the brain damage caused by COVID-19, it is still unknown, either clinically or experimentally, whether the different COVID-19 vaccine candidates can prevent SARS-CoV-2 neuroinvasion or associated damage. Here, we show that a vaccine candidate against COVID-19 based on the poxvirus MVA vector expressing the SARS-CoV-2 S protein (MVA-CoV2-S, also termed MVA-S) confers complete protection against SARS-CoV-2 neuroinvasion, preventing brain viral replication and cerebral damage. To test the efficacy of the MVA-S vaccine candidate, we used the well-established K18-hACE2 mouse model of severe COVID-19[12,13]. This transgenic mouse model has increased hACE2 cerebral expression[42], presenting significant brain permissiveness to SARS-CoV-2 replication and to the subsequent neuropathological damage. Using this COVID-19 preclinical model, we performed a thorough characterization of the spatiotemporal

SARS-CoV-2 distribution along the different brain areas. This analysis revealed that ventral areas of the brain (basal forebrain, hypothalamus and amygdala) are the first cerebral regions infected by SARS-CoV-2, with virus replication being detected at 4 dpi. On the contrary, the olfactory bulbs, which have been proposed as one of the main ports of the viral CNS entry[6,18,43], presented mild SARS-CoV-2 infection at 4 dpi, and only showed severe viral infection after 6 dpi, when SARS-CoV-2 replication has spread to most of the brain regions. Although our experimental approach was not designed to study the SARS-CoV-2 route of brain infection, these data are consistent with recent studies that fail to detect significant levels of viral replication in the olfactory bulbs of patients who died few days after viral infection[44,45]. In addition, the fact that the hypothalamus, where there are highly fenestrated blood-brain barrier capillaries[46], is one of the brain regions with the highest and earliest viral replication levels, suggests that the hematogenous is the main route of entry of SARS-CoV-2 into the CNS[47]. Another relevant finding of our analysis of SARS-CoV-2 infection in K18-hACE2 mice is that brain viral replication occurs primarily in neurons, inducing significant neuronal cell death. These findings are consistent with the detection of SARS-CoV-2 in cortical neurons from deceased COVID-19 patients and with the induction of neuronal apoptosis in infected human brain organoids[5]. Besides the neurodegeneration induced by the severe cerebral SARS-CoV-2 infection, we also detected important vascular alterations in the brains of infected K18-hACE2 mice, similar to those previously described in COVID-19 patients and preclinical models[20,48]. Nevertheless, in contrast to reported data obtained from brains of deceased COVID-19 patients[11,21] our histological analyses of $GFAP^+$-astrocytes or $IBA1^+$-microglia did not reveal a robust neuroinflammatory state in the SARS-CoV-2 infected brains. This apparent discrepancy can be explained because at the latest time

point analyzed (6 dpi) the neuroinflammatory response induced by SARS-CoV-2 infection is still in an initial stage, as can be distinguished by the higher IBA-1 expression observed in the microglial cells of the infected brains.

Our study clearly demonstrates that MVA-CoV2-S vaccination totally protects K18-hACE2 mice against SARS-CoV-2 neuroinvasion, conferring sterilizing immunity against brain viral replication and damage. In previous studies, we have reported that the MVA-CoV2-S vaccine candidate induced in mice robust SARS-CoV-2-specific humoral and cellular immune responses, producing high titers of binding IgG antibodies against the S and receptor binding domain (RBD) proteins, high titers of neutralizing antibodies able to recognize different variants of concern and potent, broad and polyfunctional S-specific T cell immune responses[35–37]. Moreover, memory SARS-CoV-2-specific humoral and cellular immune responses were detected in mice even at 6 months after the last MVA-S immunization[36]. We have also established that K18-hACE2 mice vaccinated with MVA-CoV2-S and challenged with SARS-CoV-2 are protected against mortality, body weight loss, viral lung replication and lung pathology and have reduced levels of proinflammatory cytokines, being the two doses treatment more effective that one single dose[35–37]. SARS-CoV-2 replication in K18-hACE2 mice is well described to occur primarily in lungs, during the first 2- 4 dpi, and later on the cerebral tissue, between 3-7 dpi[12,13]. Probably, the exhaustive control exerted by MVA-CoV2-S vaccination on lung viral replication during the early stage of infection prevents viral shedding to other organs, such as the brain. The fact that immunization with a single dose of MVA-CoV2-S reduces, but does not prevent virus infection in the lungs[35–37], contrasts with the complete inhibition of brain viral infection in mice vaccinated with a single dose reported here, and suggest that the block of viral brain infection could be due to the

broad specificity of the immune responses triggered by MVA-CoV2-S vaccination. This inhibition is probably the result of the combined action of SARS-CoV-2 specific neutralizing antibodies and of $CD4^+$ and $CD8^+$ T cell responses triggered by vaccination, and in turn preventing virus access to the brain.

To the best of our knowledge, only two articles have addressed the efficacy of COVID-19 vaccine candidates to protect against SARS-CoV-2 cerebral infection. In these works, the efficacy of adenoviral[49] or lentiviral[50] S-based vaccines against brain viral infection were analysed using K18-hACE2 transgenic mice, obtaining different outcomes. The adenoviral based-S vaccine candidate failed to control the brain SARS-CoV-2 replication, reducing the brain viral load only when it was combined with a nucleocapsid-based vaccine candidate; whereas the lentiviral S-based vaccine candidate was able to block cerebral SARS-CoV-2 replication. Interestingly, our MVA-CoV2-S vaccine candidate not only completely abolishes SARS-CoV-2 brain replication, even with one single dose, but also confers sustained protection against a second viral infection, being all vaccinated mice completely resistant to a SARS-CoV-2 reinfection 7 weeks after the first challenge. Interestingly, MVA-CoV2-S was able to induce memory SARS-CoV-2-specific humoral and $CD4^+$ and $CD8^+$ T cell immune responses even 6 months after the last dose[36], strengthening the potent immunogenicity and durability of this vaccine candidate.

An important aspect of our data is that MVA-CoV2-S vaccination confers complete protection against the cerebral damage induced by a severe SARS-CoV-2 infection, independently of the one or two dose vaccination regimes, with no evidence of cellular apoptosis, neuronal degeneration or vascular alterations in any of the vaccinated mice. In a very stringent COVID-19 model as the K18-hACE2 mice, where

SARS-CoV-2 neurotropism increases, most of the neuropathological alterations induced during viral infection should be produced by direct viral neuroinvasion[3,4]. Therefore, the complete protection exerted by the MVA-CoV2-S vaccine candidate against cerebral SARS-CoV-2 infection and replication should be the main cause of the lack of neuropathological signs observed in the brains of vaccinated mice. Furthermore, the cytokine/chemokine storm produced by the systemic SARS-CoV-2 infection in many COVID-19 patients has also been proposed to induce cerebral damage, producing neurological symptoms as described in CAR-T treated patients[51,52]. In this regard, we have previously reported that MVA-CoV2-S vaccination prevented the increase in pro-inflammatory cytokines induced by SARS-CoV-2 infection[36], helping to reduce the potential cytokine induced neurotoxicity in vaccinated K18-hACE2 mice.

In summary, this study shows that the MVA-CoV2-S vaccine candidate confers complete and sustained protection against SARS-CoV-2 brain infection, replication and the associated damage. These results, together with the previously described potent immunogenicity and efficacy of MVA-CoV2-S[35–37], support the evaluation of this COVID-19 vaccine candidate in clinical trials.

Methods

Ethics statement.

Transgenic K18-hACE2 female mice, expressing the human ACE2 gene, were obtained from The Jackson Laboratory [034860-B6.Cg-Tg(K18-ACE2)2Prlmn/J, genetic background C57BL/6J x SJL/J)F2]. Experiments were carried out in the biosafety level 3 (BSL-3) facilities at Centro de Investigación en Sanidad Animal (CISA)-Instituto Nacional de Investigaciones Agrarias (INIA-CSIC) (Valdeolmos, Madrid, Spain). Animal

experimentation was approved by the Ethical Committee of Animal Experimentation (CEEA) of the CNB (Madrid, Spain) and by the Division of Animal Protection of the Comunidad de Madrid (PROEX 49/20, 169.4/20 and 161.5/20). All animal procedures were performed according to the European Directive 2010/63/EU and the Spanish RD/53/2013 for the protection of animals used for scientific purposes.

Viruses.

The poxviruses used in this study included the attenuated MVA-WT strain obtained from the Chorioallantois vaccinia virus Ankara (CVA) strain after 586 serial passages in chicken embryo fibroblasts (CEF)[53], and the MVA-CoV2-S vaccine candidate expressing a human codon optimized full-length SARS-CoV-2 S protein[35].

SARS-CoV-2 strain MAD6 (kindly provided by José M. Honrubia and Luis Enjuanes, CNB-CSIC, Madrid, Spain) is a virus collected from a nasopharyngeal swab from a 69-year-old male COVID-19 patient from Hospital 12 de Octubre, Madrid, Spain[54]. Growth and titration of SARS-CoV-2 MAD6 isolate has been previously described[35,36]. The full-length virus genome was sequenced and found to be identical to the SARS-CoV-2 reference sequence (Wuhan-Hu-1 isolate, GenBank: MN908947), except for the silent mutation C3037>T, and two mutations leading to amino acid changes: C14408>T (in nsp12) and A23403>G (D614G in S protein).

MVA-CoV2-S vaccination and SARS-CoV-2 infection in K18-hACE2 mice.

For experiments analyzing SARS-CoV-2 brain infection and neuropathological damage, female K18-hACE2 mice (4-5 months old; n=11) were infected with SARS-CoV-2 [MAD6 strain; 1 x 10^5 PFU in 50 µl of phosphate buffered saline (PBS); intranasally (i.n.)] as

previously described[35,36] .Uninfected control mice only received 50 µl of PBS by i.n. route. Mice were sacrificed at 2 (n=3), 4 (n=3) and 6 (n=5) dpi, brains were extracted and fixed in 4% paraformaldehyde (PFA; Sigma-Aldrich) in PBS for at least 7 days.

MVA-CoV2-S immunization studies were carried out as previously indicated[35,36] . Briefly, in the experiments of a single SARS-CoV-2 infection female K18-hACE2 mice (10 weeks old; n=11 per group) received one or two doses of 1 x 10^7 PFU of MVA-CoV2-S in 100 µl of PBS (i.m.; 50 µl/leg) at 0 and 4 weeks. Also, mice primed and boosted with non-recombinant MVA-WT were used as control group. At week 9, mice were challenged with SARS-CoV-2 as specified above. For the reinfection experiments, MVA-S vaccinated mice were additionally re-infected with SARS-CoV-2 (MAD6 strain; 1 x 10^5 PFU in 50 µl of PBS; i.n.) 7 weeks after the first viral infection[36]. In this second set of experiments, mice treated with non-recombinant MVA-WT and nonvaccinated SARS-CoV-2 infected mice were used as controls. Mice were sacrificed at 4 (n=3) and 6 (n=5) dpi, for single SARS-CoV-2 infection and for reinfection experiments, respectively. Subsequently, the brains were extracted and fixed in 4% PFA for a period longer than 7 days.

Histological staining.

Brains were cryoprotected in 30% sucrose (Sigma-Aldrich) in PBS and included in Optimum Cutting Temperature compound (O.C.T. compound, Tissue-Tek). Coronal sections (thickness 40 µm) were cut on a cryostat (Leica). SARS-CoV-2 N protein, NeuN, c-casp3, GFAP, IBA1 and IB4 immunohistological detection were performed as previously described[40,55–57] using, respectively, mouse monoclonal anti-SARS-CoV-2 (1:100, Invitrogen, Cat. #MA1-704); anti-NeuN (rabbit polyclonal, 1:500, Millipore, Cat.# ABN78; and mouse monoclonal, 1:200, Millipore, Cat.# MAB377, 1:200); rabbit

polyclonal anti-c-casp3 (1:100, Cell Signaling, Cat.# 9661); polyclonal anti-GFAP (rabbit polyclonal, 1:500, Dako, Cat.# Z0334; and mouse monoclonal, 1:2000, Sigma Cat.# G3893); anti-IBA1 (rabbit polyclonal 1:500; Wako Chemicals, Cat.# 019-19741; and rabbit polyclonal, 1:1000, Synaptic System, Cat.# 234003); anti-IB4 (biotinylated isolectin B4, 1:50; Sigma Cat.# L2140), and secondary peroxidase-conjugated antibody kits (NeoBiotech, Cat.# NB-23-00029-1; NB-23-00030-1) or fluorescence secondary antibodies (Goat-anti-Mouse Alexa488, 1:400, Jackson ImmunoResearch, Cat.# 115-545-003; goat-anti-Rabbit Alexa647, 1:400, Jackson ImmunoResearch Cat.# 111-605-003; goat-anti-Rabbit Alexa568, 1:400, Invitrogen, Cat.# A-11011; Streptoavidin-Cy3, 1:500; and Jackson ImmunoResearch, Cat.# 016-160-084). In the case of SARS-CoV-2 and c-casp3 staining brain sections were subjected to citrate antigen retrieval [sodium citrate 10mM (Sigma-Aldrich), pH: 6.0; 15 min 97ºC]; also for SARS-CoV-2 immunodetection brain sections were treated with mouse on mouse blocking reagent (Vector; Cat.# MKB2213-1). In immunofluorescence experiments, nuclei were stained with DAPI (1:1000, Sigma-Aldrich). Nissl staining was performed as previously described[58].

Image analysis and stereology.

Image acquisition and analysis were performed with light transmitted (Olympus, AX70 or Bx61, both with digital refrigerated camera DP72) or confocal microscopes (Nikon, A1R$^+$; or Leica, Stellaris 8 Scan Head) and their specific imaging software. Qualitative analysis of SARS-CoV-2 infection was performed by two independent blind researchers. Imaging analyses of c-casp3, IBA1 and IB4 were carried out as previously indicated[40,56,57] using FIJI software (National Institutes of Health, USA). NeuN$^+$ and Nissl$^+$ neuronal

density was estimated by systematic random sampling using the optical dissector method[59]. Briefly, reference volumes were outlined at low magnification (4x) and neurons were counted at high magnification (40x) using a 4900 x 30 μm^2 optical dissector with a guard volume of 5 μm to avoid artefacts on the cut surface of the sections. All stereological procedures were performed using the New CAST™ system (Visiopharm) as previously described[55,58].

Analysis of SARS-CoV-2 RNA by quantitative RT-PCR.

The region corresponding to the cingulate cortex (Bregma: +1.42 to -0.10 mm) and the hypothalamus (Bregma: -1.82 to -2.18 mm) were microdissected from 3 coronal histological sections (thickness 40 μm) under a stereoscopic binocular microscope (Olympus SZX16), according to the mouse brain stereotaxic atlas[60]. RNA was isolated using RecoverAll™ Total Nucleic Acid Isolation Kit (Invitrogen, Cat.# AM1975) following the manufacturer's instructions. Concentration and purity of the total RNA samples were measured using the NanoDrop 2000 Spectrophotometer (ThermoFisher Scientific). RNA integrity was assessed using Agilent 2100 Bioanalyzer and the RNA 6000 LabChip kit (Agilent Technologies, Cat.# 5067-1511). For cDNA synthesis, 1 μg of RNA was reverse-transcribed by QuantiTect Reverse Transcription Kit (Qiagen, Cat.# 205311), according to the manufacturer's specifications.

SARS-CoV-2 viral RNA content was determined using previously validated set of primers and probes specific for the SARS-CoV-2 subgenomic RNA for the protein E[61] and cellular 18S rRNA for normalization (Thermo Fisher scientific, Cat.# 4333760F). Data were acquired with a 7500 real-time PCR system and analyzed with 7500 software v2.0.6 (Applied Biosystems). Relative RNA arbitrary units (a.u.) were quantified relative to the

476 negative group (uninfected K18-hACE2 mice) and were performed using the $2^{-\Delta\Delta Ct}$
477 method. All samples were tested in triplicate.
478
479 **Statistical analysis.**
480 The number of mice analyzed in each experimental group and the statistical tests
481 applied are indicated in each figure legend. Data are presented as mean ± standard error
482 of the mean (SEM). In all cases, normality and equal variance tests were performed and,
483 when passed, the ANOVA test with Dunnett, Tukey, Friedman or Fisher LSD post hoc
484 analysis for multiple group comparisons was carried out. In the cases where normality
485 or homoscedasticity tests failed, the non-parametric Kruskal-Wallis H with post hoc
486 Dunn´s test was performed. All statistical analyses were conducted using Prism 8.0
487 (GraphPad Software).
488
489 **Data availability.**
490 All relevant data are included in the paper. This study did not generate data sets
491 deposited in external repositories. Information/data required will be available by the
492 corresponding authors upon request.
493
494 **Acknowledgments**
495 The authors thank the Centro de Investigación en Sanidad Animal (CISA)-Instituto
496 Nacional de Investigaciones Agrarias (INIA-CSIC) (Valdeolmos, Madrid, Spain) for the
497 BSL-3 facilities. SARS-CoV-2 MAD6 virus isolate was kindly provided by José M. Honrubia
498 and Dr. Luis Enjuanes (CNB-CSIC, Madrid, Spain). We also thank to Dr. Konstantin L.
499 Levitsky for excellent technical assistance with the confocal acquisition. We thank the

Spanish Research Council (CSIC) and the Spanish Ministry of Science and Innovation (MICINN) for continuous support.

This research was supported by MCIN/Spanish Research Agency (AEI)/ 10.13039/501100011033 grants: PID2019-105995RB-I00 (J.T.-A. and J.V.), PID2020-114481RB-I00 (J.G.-A. and M.E.), and PID2019-106410RB-I00 (J.L.-B.). Moreover, this research work was also funded by Red TerCel ISCIII, RD16/0011/0025 (J.T.-A.); Consejería de Salud y Familias, Junta de Andalucía Grant, PECOVID-0078-2020 (R.R.-L. and J.V.); Fondo COVID-19 grant COV20/00151 [Spanish Health Ministry, Instituto de Salud Carlos III (ISCIII)], Fondo Supera COVID-19 (Crue Universidades-Banco Santander) grant and CSIC grant 202120E079 (J.G.-A.); and CSIC grant 2020E84, La CaixaImpulse grant CF01-00008, Ferrovial and MAPFRE donations (M.E.). Additionally, we have also funding from the European Commission-NextGenerationEU, through CSIC's Global Health Platform (PTI Salud Global) (J.G.-A. and M.E.) and the European Research Council (ERC Advanced Grant PRJ201502629) (J.L.-B.).

Authors' contributions

Conceptualization: J.V., J.G.-A., M.E, J.L.B and J.T.-A. Funding acquisition: J.V., J.G.-A., R.R.-L., M.E., J.L.-B. and J.T.-A. Methodology and investigation: J.V., J.G.-A., R.R.-L., D.C.-R., M.A.-V., F.C.-F., R.G.-S., E.G.-R., J.L.-O., C.Z., D.A., P.P., A.R.-N., A.M.-C., Data analysis: J.V., A.M.-C., A.P. Project supervision: J.V., J.G.-A., M.E, J.L.-B and J.T.-A. Visualization: J.V., A.M.-C., A.P. Writing—original draft: J.V. and J.T.-A. Writing—review and editing: J.V., J.G.-A., R.G.-S., A.M.-C., A.P., M.E., J.L.-B. and J.T.-A. All authors have read and agreed to the published version of the manuscript.

Conflict of interest

The authors declare that they have no conflict of interest.

References

1. Wu, F. *et al.* A new coronavirus associated with human respiratory disease in China. *Nature* **579**, 265–269 (2020).
2. Gupta, A. *et al.* Extrapulmonary manifestations of COVID-19. *Nature Medicine* **26**, 1017–1032 (2020).
3. Song, E. *et al.* Neuroinvasion of SARS-CoV-2 in human and mouse brain. *Journal of Experimental Medicine* **218**, e20202135 (2021).
4. Kumari, P. *et al.* Neuroinvasion and Encephalitis Following Intranasal Inoculation of SARS-CoV-2 in K18-hACE2 Mice. *Viruses* **13**, 132- (2021).
5. Ramani, A. *et al.* SARS -CoV-2 targets neurons of 3D human brain organoids. *The EMBO Journal* **39**, e106230 (2020).
6. Dias de Melo, G. *et al.* COVID-19-related anosmia is associated with viral persistence and inflammation in human olfactory epithelium and brain infection in hamsters. *Science Translational Medicine* **13**, eabf8396 (2021).
7. Arbour, N., Day, R., Newcombe, J. & Talbot, P. J. Neuroinvasion by Human Respiratory Coronaviruses. *Journal of Virology* **74**, 8913–8921 (2000).
8. Netland, J., Meyerholz, D. K., Moore, S., Cassell, M. & Perlman, S. Severe Acute Respiratory Syndrome Coronavirus Infection Causes Neuronal Death in the Absence of Encephalitis in Mice Transgenic for Human ACE2. *Journal of Virology* **82**, 7264–7275 (2008).
9. Li, K. *et al.* Middle East Respiratory Syndrome Coronavirus Causes Multiple Organ Damage and Lethal Disease in Mice Transgenic for Human Dipeptidyl Peptidase 4. *The Journal of Infectious Diseases* **213**, 712–722 (2016).
10. Lewis, A. *et al.* Cerebrospinal fluid in COVID-19: A systematic review of the literature. *Journal of the Neurological Sciences* **421**, 117316 (2021).
11. Matschke, J. *et al.* Neuropathology of patients with COVID-19 in Germany: a post-mortem case series. *The Lancet Neurology* **19**, 919–929 (2020).
12. Winkler, E. S. *et al.* SARS-CoV-2 infection of human ACE2-transgenic mice causes severe lung inflammation and impaired function. *Nature Immunology* **21**, 1327–1335 (2020).
13. Oladunni, F. S. *et al.* Lethality of SARS-CoV-2 infection in K18 human angiotensin-converting enzyme 2 transgenic mice. *Nature Communications* **11**, 6122 (2020).
14. Zhou, B. *et al.* SARS-CoV-2 spike D614G change enhances replication and transmission. *Nature* **592**, 122–127 (2021).
15. Imai, M. *et al.* Syrian hamsters as a small animal model for SARS-CoV-2 infection and countermeasure development. *Proceedings of the National Academy of Sciences of the United States of America* **117**, 16587–16595 (2020).
16. Schlottau, K. *et al.* SARS-CoV-2 in fruit bats, ferrets, pigs, and chickens: an experimental transmission study. *The Lancet Microbe* **1**, e218–e225 (2020).

17. Philippens, I. H. C. H. M. *et al.* SARS-CoV-2 causes brain inflammation and induces Lewy body formation in macaques. *bioRxiv* (2021) doi:10.1101/2021.02.23.432474.
18. Jiao, L. *et al.* The olfactory route is a potential way for SARS-CoV-2 to invade the central nervous system of rhesus monkeys. *Signal Transduction and Targeted Therapy* **6**, 169 (2021).
19. Yang, A. C. *et al.* Dysregulation of brain and choroid plexus cell types in severe COVID-19. *Nature* **595**, 565–571 (2021).
20. Wenzel, J. *et al.* The SARS-CoV-2 main protease Mpro causes microvascular brain pathology by cleaving NEMO in brain endothelial cells. *Nature Neuroscience* **24**, 1522–1533 (2021).
21. Schwabenland, M. *et al.* Deep spatial profiling of human COVID-19 brains reveals neuroinflammation with distinct microanatomical microglia-T cell interactions. *Immunity* **54**, 1594–1610 (2021).
22. Kanberg, N. *et al.* Neurochemical evidence of astrocytic and neuronal injury commonly found in COVID-19. *Neurology* **95**, e1754–e1759 (2020).
23. Ameres, M. *et al.* Association of neuronal injury blood marker neurofilament light chain with mild-to-moderate COVID-19. *Journal of Neurology* **267**, 3476–3478 (2020).
24. Nalbandian, A. *et al.* Post-acute COVID-19 syndrome. *Nature Medicine* **27**, 601–615 (2021).
25. Heneka, M. T., Golenbock, D., Latz, E., Morgan, D. & Brown, R. Immediate and long-term consequences of COVID-19 infections for the development of neurological disease. *Alzheimer's Research and Therapy* **12**, (2020).
26. Fernández-Castañeda, A. *et al.* Mild respiratory SARS-CoV-2 infection can cause multi-lineage cellular dysregulation and myelin loss in the brain Equal contribution. *bioRxiv* (2022) doi:10.1101/2022.01.07.475453.
27. Baden, L. R. *et al.* Efficacy and Safety of the mRNA-1273 SARS-CoV-2 Vaccine. *New England Journal of Medicine* **384**, 403–416 (2021).
28. Polack, F. P. *et al.* Safety and Efficacy of the BNT162b2 mRNA Covid-19 Vaccine. *New England Journal of Medicine* **383**, 2603–2615 (2020).
29. Voysey, M. *et al.* Safety and efficacy of the ChAdOx1 nCoV-19 vaccine (AZD1222) against SARS-CoV-2: an interim analysis of four randomised controlled trials in Brazil, South Africa, and the UK. *The Lancet* **397**, 99–111 (2021).
30. Sadoff, J. *et al.* Safety and Efficacy of Single-Dose Ad26.COV2.S Vaccine against Covid-19. *New England Journal of Medicine* **384**, 2187–2201 (2021).
31. Logunov, D. Y. *et al.* Safety and immunogenicity of an rAd26 and rAd5 vector-based heterologous prime-boost COVID-19 vaccine in two formulations: two open, non-randomised phase 1/2 studies from Russia. *The Lancet* **396**, 887–897 (2020).
32. al Kaabi, N. *et al.* Effect of 2 Inactivated SARS-CoV-2 Vaccines on Symptomatic COVID-19 Infection in Adults: A Randomized Clinical Trial. *JAMA - Journal of the American Medical Association* **326**, 35–45 (2021).
33. Keehner, J. *et al.* SARS-CoV-2 Infection after Vaccination in Health Care Workers in California. *New England Journal of Medicine* **384**, 1774–1775 (2021).

34. Levine-Tiefenbrun, M. *et al.* Initial report of decreased SARS-CoV-2 viral load after inoculation with the BNT162b2 vaccine. *Nature Medicine* **27**, 790–792 (2021).
35. García-Arriaza, J. *et al.* COVID-19 Vaccine Candidates Based on Modified Vaccinia Virus Ankara Expressing the SARS-CoV-2 Spike Protein Induce Robust T- and B-Cell Immune Responses and Full Efficacy in Mice. *Journal of Virology* **95**, (2021).
36. Lázaro-Frías, A. *et al.* Full efficacy and long-term immunogenicity induced by the SARS-CoV-2 vaccine candidate MVA-CoV2-S in mice. *NPJ Vaccines* **In press**, (2022).
37. Pérez, P. *et al.* A Single Dose of an MVA Vaccine Expressing a Prefusion-Stabilized SARS-CoV-2 Spike Protein Neutralizes Variants of Concern and Protects Mice From a Lethal SARS-CoV-2 Infection. *Frontiers in Immunology* **12**, 824728 (2022).
38. Zheng, J. *et al.* COVID-19 treatments and pathogenesis including anosmia in K18-hACE2 mice. *Nature* **589**, 603–607 (2021).
39. Heine, V. M., Maslam, S., Zareno, J., Joëls, M. & Lucassen, P. J. Suppressed proliferation and apoptotic changes in the rat dentate gyrus after acute and chronic stress are reversible. *European Journal of Neuroscience* **19**, 131–144 (2004).
40. Alvarez-Vergara, M. I., Rosales-Nieves, A. E. & March-Díaz, R. Non-productive angiogenesis disassembles Aß plaque-associated blood vessels. *Nature Communications* **12**, 3098 (2021).
41. Ellul, M. A. *et al.* Neurological associations of COVID-19. *The Lancet Neurology* **19**, 767–783 (2020).
42. McCray, P. B. *et al.* Lethal Infection of K18-hACE2 Mice Infected with Severe Acute Respiratory Syndrome Coronavirus. *Journal of Virology* **81**, 813–821 (2007).
43. Meinhardt, J. *et al.* Olfactory transmucosal SARS-CoV-2 invasion as a port of central nervous system entry in individuals with COVID-19. *Nature Neuroscience* **24**, 168–175 (2021).
44. Khan, M. *et al.* Visualizing in deceased COVID-19 patients how SARS-CoV-2 attacks the respiratory and olfactory mucosae but spares the olfactory bulb. *Cell* **184**, 5932–5949 (2021).
45. Butowt, R., Meunier, N., Bryche, B. & von Bartheld, C. S. The olfactory nerve is not a likely route to brain infection in COVID-19: a critical review of data from humans and animal models. *Acta Neuropathologica* **141**, 809–822 (2021).
46. Haddad-Tóvolli, R., Dragano, N. R. V., Ramalho, A. F. S. & Velloso, L. A. Development and function of the blood-brain barrier in the context of metabolic control. *Frontiers in Neuroscience* **11**, 224 (2017).
47. Krasemann, S. *et al.* The blood-brain barrier is dysregulated in COVID-19 and serves as a CNS entry route for SARS-CoV-2. *Stem Cell Reports* (2022) doi:10.1016/J.STEMCR.2021.12.011.
48. Kurki, S. N. *et al.* APOE ε4 associates with increased risk of severe COVID-19, cerebral microhaemorrhages and post-COVID mental fatigue: a Finnish biobank, autopsy and clinical study. *Acta Neuropathologica Communications* **9**, 199 (2021).

49. Dangi, T., Class, J., Palacio, N., Richner, J. M. & Penaloza MacMaster, P. Combining spike- and nucleocapsid-based vaccines improves distal control of SARS-CoV-2. *Cell Reports* **36**, (2021).
50. Ku, M. *et al.* Brain cross-protection against SARS-CoV-2 variants by a lentiviral vaccine in new transgenic mice. *EMBO Molecular Medicine* **13**, e14459 (2021).
51. Thepmankorn, P. *et al.* Cytokine storm induced by SARS-CoV-2 infection: The spectrum of its neurological manifestations. *Cytokine* **138**, 155404 (2021).
52. Brudno, J. N. & Kochenderfer, J. N. Recent advances in CAR T-cell toxicity: Mechanisms, manifestations and management. *Blood Reviews* **34**, 45–55 (2019).
53. Mayr, A., Stickl, H., Müller, H., Danner, K. & Singer, H. The smallpox vaccination strain MVA: marker, genetic structure, experience gained with the parenteral vaccination and behavior in organisms with a debilitated defence mechanism (author's transl). *Zentralbl Bakteriol B* . **167**, 375–390 (1978).
54. Díez, J. M. *et al.* Cross-neutralization activity against SARS-CoV-2 is present in currently available intravenous immunoglobulins. *Immunotherapy* **12**, 1247–1255 (2020).
55. Villadiego, J. *et al.* Long-term immunosuppression for CNS mouse xenotransplantation: Effects on nigrostriatal neurodegeneration and neuroprotective carotid body cell therapy. *Xenotransplantation* **25**, e12410 (2018).
56. Cabello-Rivera, D., Sarmiento-Soto, H., López-Barneo, J. & Muñoz-Cabello, A. M. Mitochondrial complex I function is essential for neural stem/progenitor cells proliferation and differentiation. *Frontiers in Neuroscience* **13**, 664 (2019).
57. March-Diaz, R. *et al.* Hypoxia compromises the mitochondrial metabolism of Alzheimer's disease microglia via HIF1. *Nature Aging* **1**, 385–399 (2021).
58. Muñoz-Manchado, A. B. *et al.* Chronic and progressive Parkinson's disease MPTP model in adult and aged mice. *Journal of Neurochemistry* **136**, 373–387 (2016).
59. West, M. J. New stereological methods for counting neurons. *Neurobiology of Aging* **14**, 275–285 (1993).
60. Paxinos, G. & Franklin, K. B. J. *The Mouse Brain in Stereotaxic Coordinates*. (Academic Press, 1997).
61. Corman, V. M. *et al.* Detection of 2019 novel coronavirus (2019-nCoV) by real-time RT-PCR. *Eurosurveillance* **25**, 2000045 (2020).

Figures

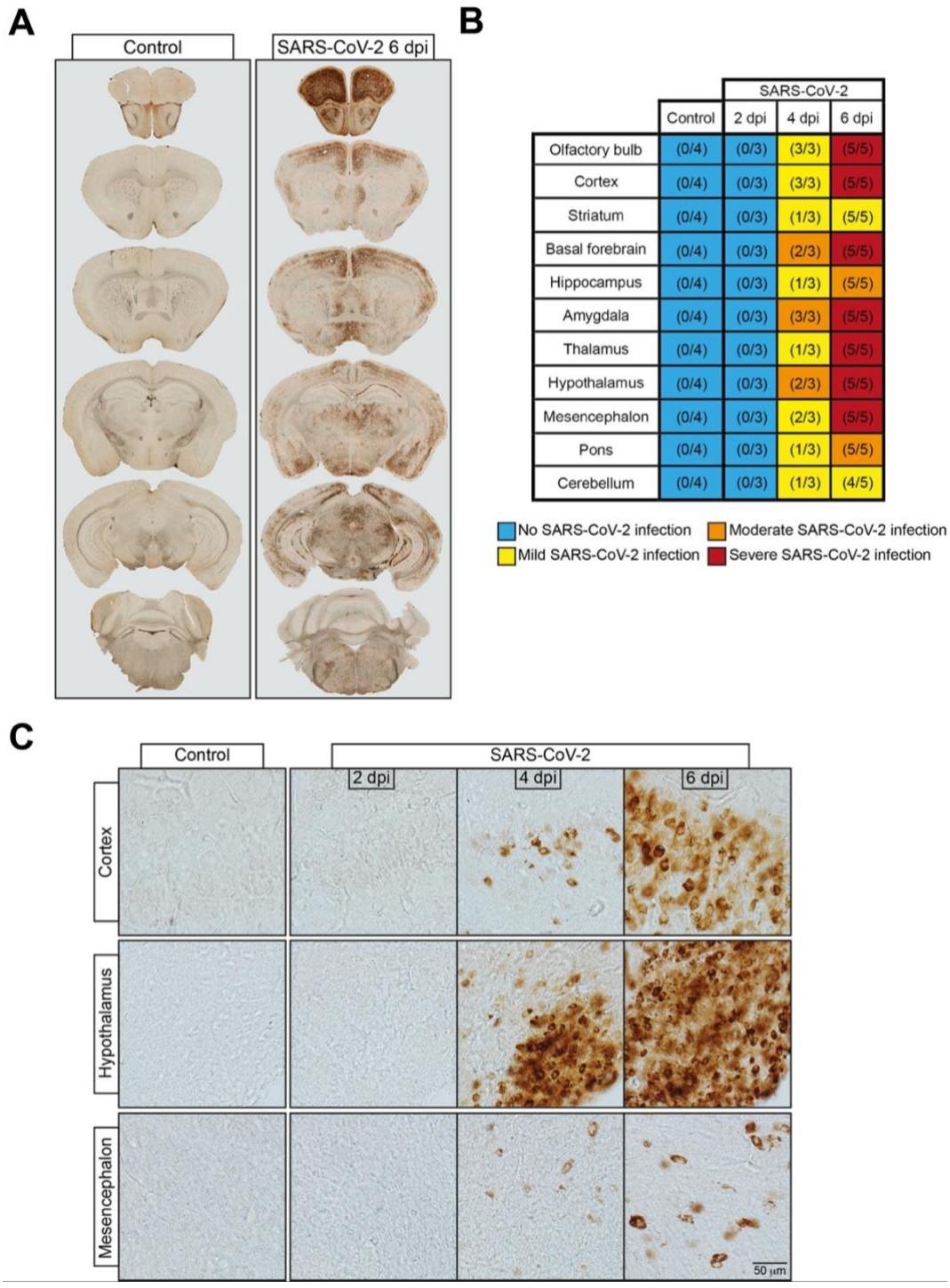

Figure 1. Analysis of SARS-CoV-2 brain infection in K18-hACE2 mice. A. Brain coronal sections of control (uninfected) and SARS-CoV-2 infected K18-hACE2 mice (6 dpi) after immunohistochemistry against the SARS-CoV-2 N protein. B. Qualitative analysis of SARS-CoV-2 level of infection in different cerebral regions of infected K18-hACE2 mice at 2, 4, and 6 dpi. Between brackets the number of mice showing SARS-CoV-2$^+$ cells among the total number of mice studied is indicated for each brain region analyzed. C. High magnification images, after SARS-CoV-2 N immunohistochemistry, illustrating the time course of SARS-CoV-2 infection in the cortex, hypothalamus and mesencephalon of control and infected K18-hACE2 mice.

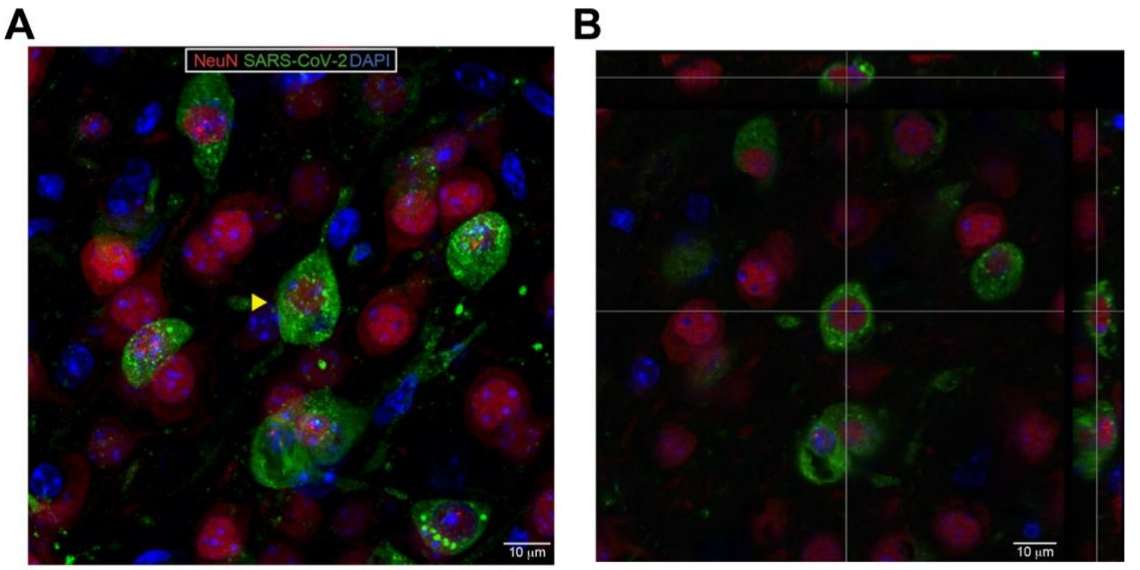

Figure 2. Neuronal replication of SARS-CoV-2 in K18-hACE2 mice. A. High resolution Z-projection confocal images of the cortex of SARS-CoV-2 infected K18-hACE2 mice, after SARS-CoV-2 (green) and NeuN (red) immunofluorescence detection, showing specific strong viral load in neuronal cells. B. Orthogonal projection of the cortical neuron pointed by an arrowhead in A, demonstrating the colocalization of the cytoplasmic SARS-CoV-2 and nuclear NeuN signals in the same neuronal cell. Nuclei were counterstained with DAPI (blue).

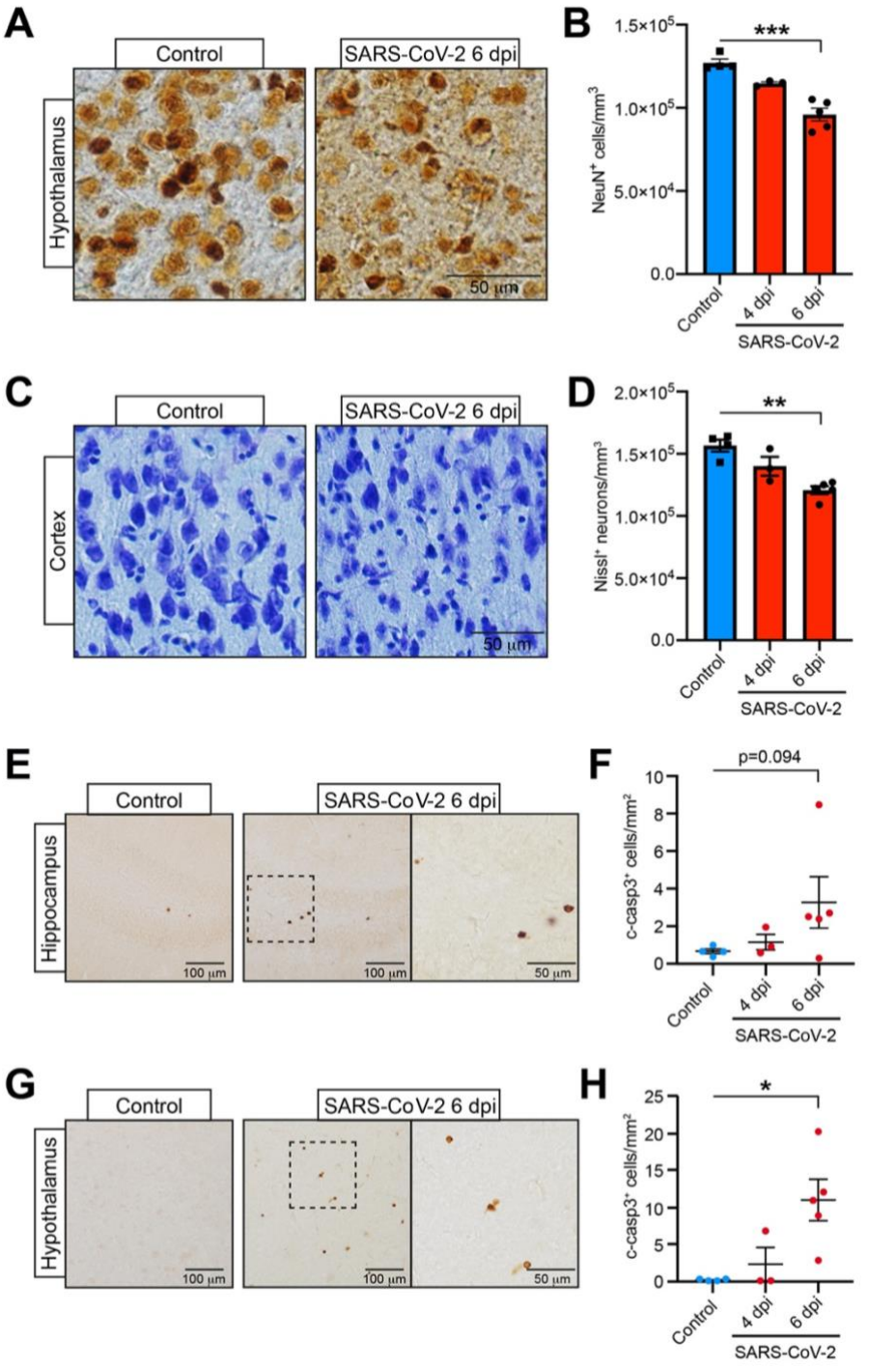

Figure 3. SARS-CoV-2 brain infection produces neuronal cell death. A-D. Light-transmitted images of hypothalamic NeuN$^+$ (A) and cortical Nissl$^+$ (C) neurons of control and SARS-CoV-2 infected mice, and stereological quantification of neuronal density in these areas (B and D). E-H. Hippocampal (E) and hypothalamic (G) images from control and SARS-CoV-2 infected mice after immunohistochemistry against apoptotic c-caspase 3. Images in the right column depict, at higher magnification, the insets of the central column. F and H. Quantification of the density of c-caspase 3$^+$ cells in the hippocampus (F) and hypothalamus (H). B,D,F,H. Data are presented as mean ± standard error of the mean (S.E.M.). Controls, n=4; SARS-CoV-2: 4 dpi, n=3; and 6 dpi, n=5 mice. ANOVA, post hoc Dunnett's (B) or Fisher's LSD (D, F) test; and Kruskal-Wallis test, post hoc Dunn´s test (H). *p<0.05; **p<0.01; ***p<0.01.

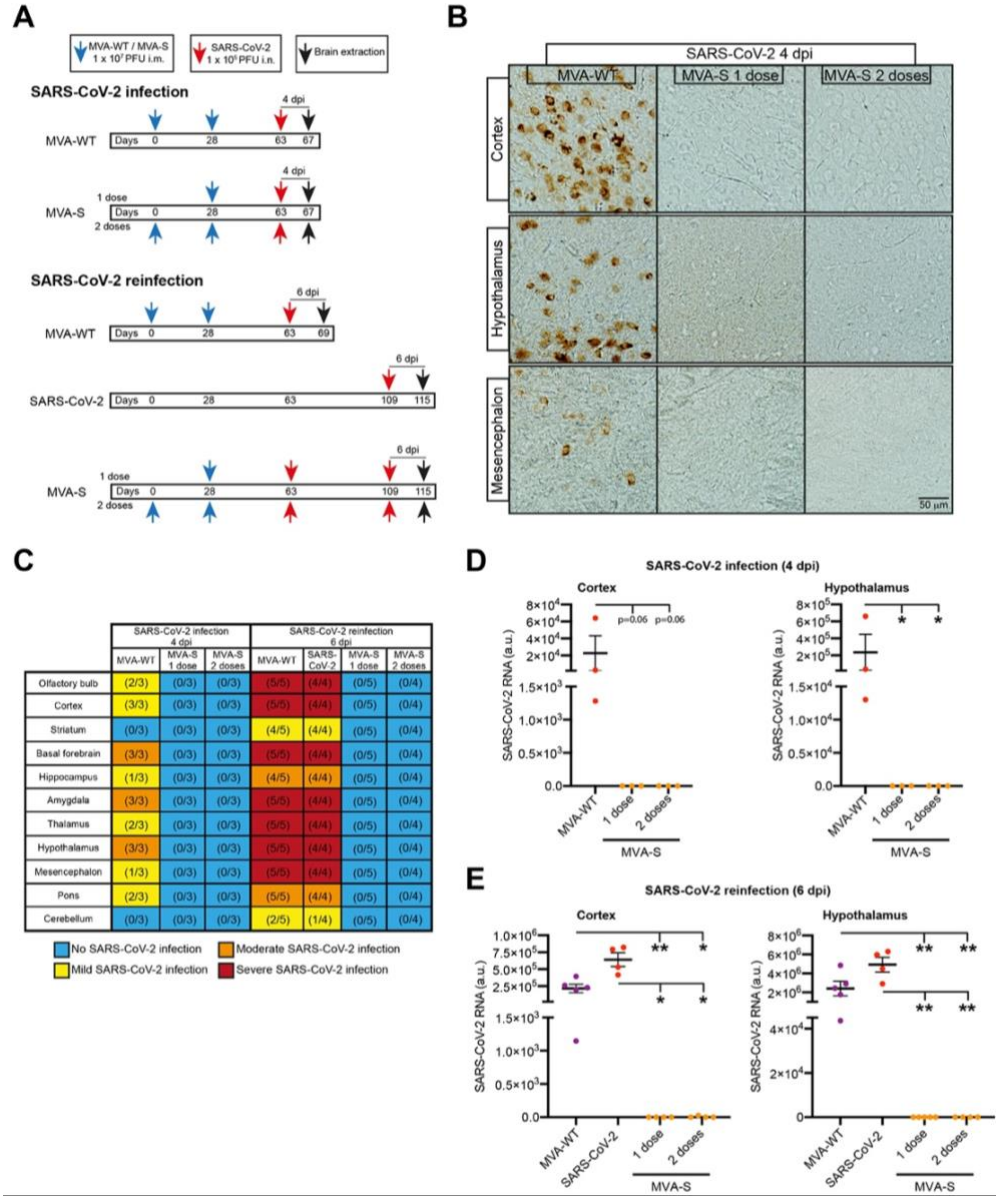

730

731 **Figure 4. MVA-CoV2-S vaccination prevents SARS-CoV-2 brain infection.** A. Schematic diagram
732 showing the schedule used to analyze the protection induced by MVA-CoV2-S vaccination
733 against SARS-CoV-2 brain infection in K18-hACE2 mice. Note that MVA-CoV2-S was tested for a
734 single SARS-CoV-2 infection (top diagrams, brain extraction at 4 dpi) or for a second reinfection
735 (bottom diagrams, brain extraction at 6 dpi). B. High magnification images from the cortex,
736 hypothalamus and mesencephalon after SARS-CoV-2 N immunohistochemistry, illustrating the
737 efficacy of the MVA-S vaccine candidate, in a regimen of 1 or 2 doses, against SARS-CoV-2
738 cerebral infection. C. Qualitative analysis of the level of SARS-CoV-2 infection in the different
739 cerebral regions of the experimental groups showed in A. Between brackets the number of mice
740 showing SARS-CoV-2$^+$ cells among the total number of mice studied is indicated for each brain
741 region analyzed. D-E. Quantitative analysis of SARS-CoV-2 RNA detected by RT-qPCR targeting
742 the viral E gene, in the cortex and hypothalamus, of the experimental groups described
743 previously for the SARS-CoV-2 infection (D) or reinfection (E) experiments. Data are presented
744 as mean ± SEM. SARS-CoV-2 infection experiment (4 dpi): n=3 per experimental group. SARS-
745 CoV-2 reinfection experiment (6 dpi): MVA-WT, n=5; SARS-CoV-2, n=4; MVA-S 1 dose, n=5; MVA-
746 S 2 doses, n=4. ANOVA, post hoc Friedman test (D) or Kruskal-Wallis; post hoc Dunn's test (E).
747 *p<0.05; **p<0.01.

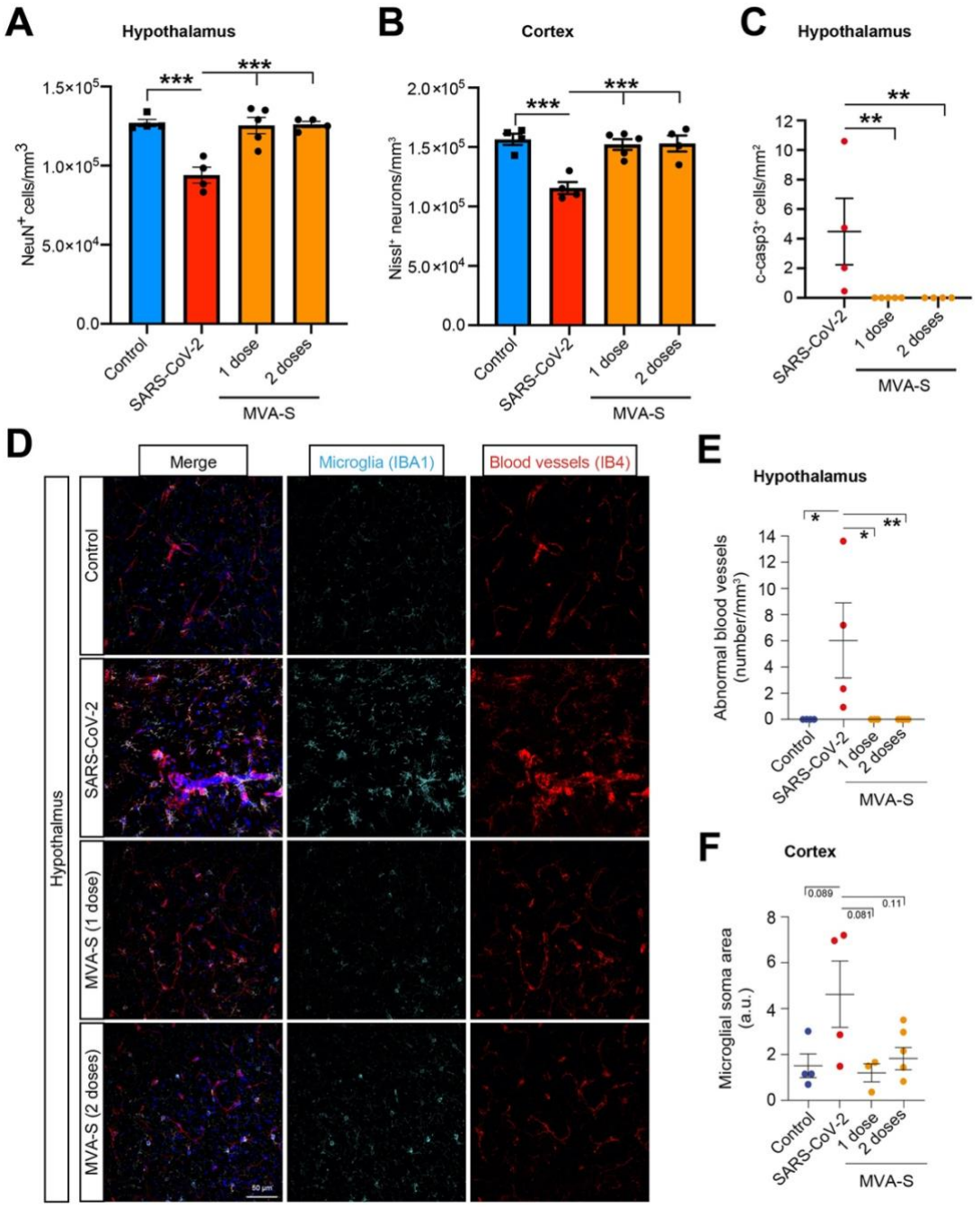

748

749 **Figure 5. MVA-CoV2-S vaccination confers protection against brain damage induced by SARS-**
750 **CoV-2 infection.** A,B. Stereological estimation of hippocampal NeuN$^+$ (A) and cortical Nissl$^+$ (B)
751 from controls (uninfected) and the experimental groups of the reinfection experiment (6 dpi):
752 SARS-CoV-2 and MVA-S, 1 and 2 doses. C. Quantification of apoptotic c-caspase 3$^+$ cells in the
753 hypothalamus of SARS-CoV-2 and MVA-S (1 or 2 doses) mice used in the reinfection experiment.
754 D. Confocal Z-projection images from the experimental groups described above, which were
755 stained with microglial (IBA1; cyan), and vascular (IB4; red) markers. Nuclei were counterstained
756 with DAPI (blue) in merge images. E. Quantification of abnormal blood vessel density in the
757 hypothalamus. F. Analysis of microglial soma area, by measurements of IBA1$^+$ optical density, in
758 the cortex (a.u.: arbitrary units). Data are presented as mean ± SEM. Controls, n=4; SARS-CoV-2,
759 n=4; MVA-S: 1 dose, n=5; 2 doses, n=4. ANOVA, post hoc Dunnett's (A) or Fisher's LSD (B), or
760 Tukey's (F) test; and Kruskal-Wallis, post hoc Dunn´s test (C,E). *p<0.05; **p<0.01; ***p<0.01.

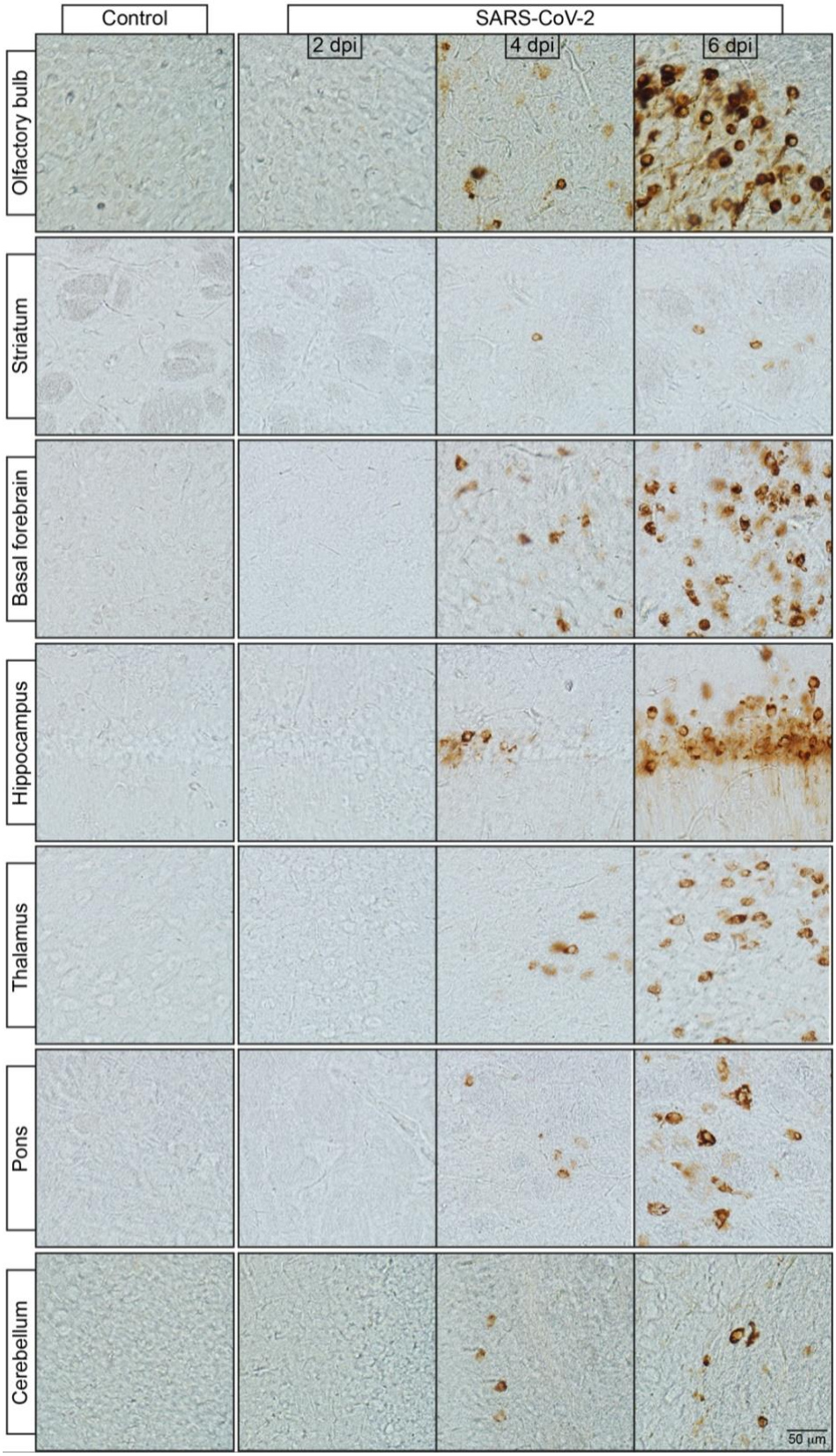

Supplementary Figure 1. Analysis of SARS-CoV-2 infection in the principal brain regions of K18-hACE2 mice. High magnification images, after SARS-CoV-2 N immunohistochemistry, from control and SARS-CoV-2 infected K18-hACE2 mice (at 2, 4 and 6 dpi) of the indicated cerebral regions showing the level of SARS-CoV-2 infection.

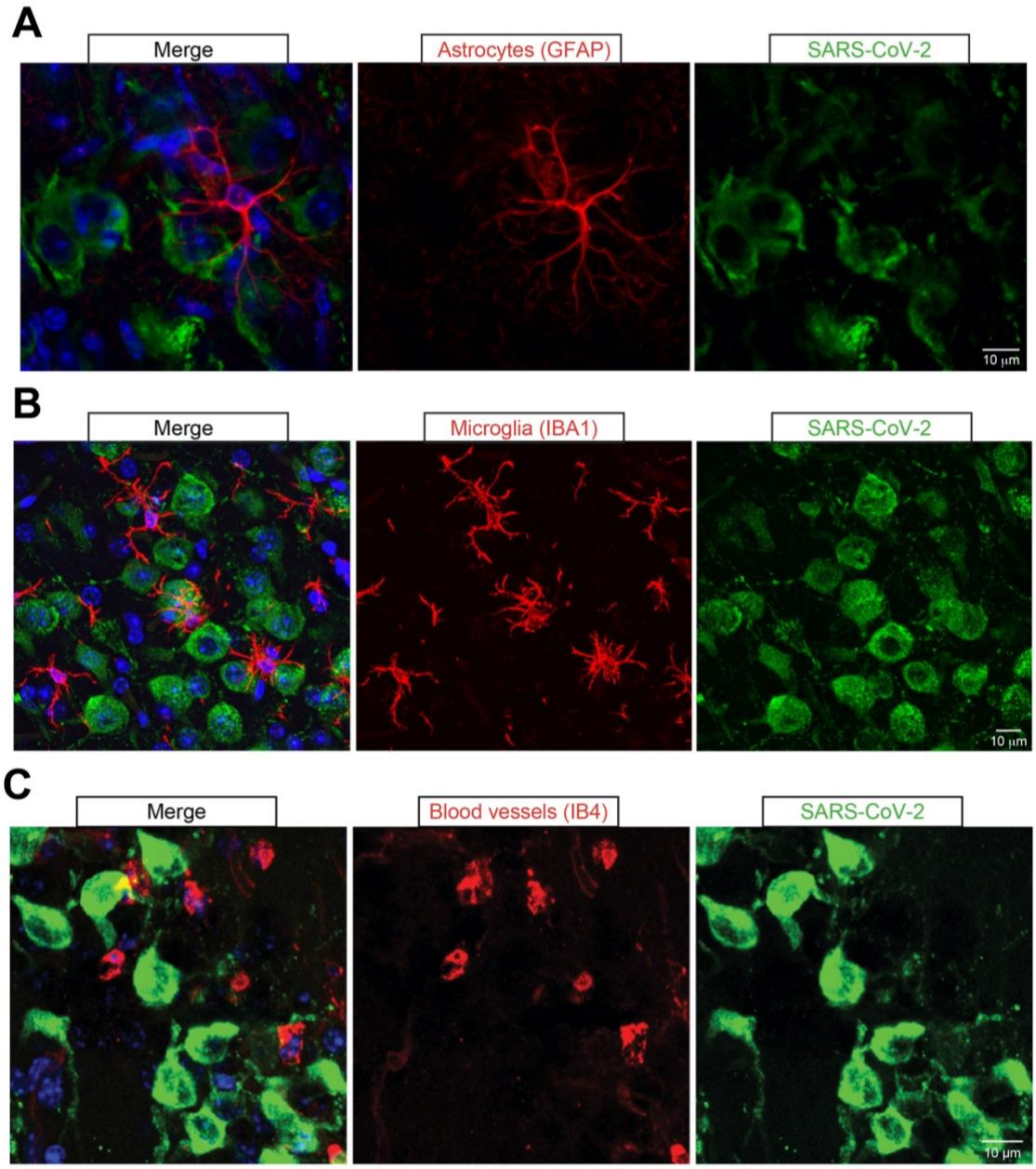

Supplementary Figure 2. Absence of significant SARS-CoV-2 replication in glial or vascular brain cells. A-B. High-resolution Z-projection confocal images from the cortex of a SARS-CoV-2 infected K18-hACE2 mouse (6 dpi), after immunohistological detection of SARS-CoV-2 N protein (green in A,B); GFAP (red in A) and IBA1 (red in B), showing the absence of SARS-CoV-2$^+$ staining in a GFAP$^+$ astrocyte (A) or IBA1$^+$ microglial cells (B). C. Cortical confocal images from a SARS-CoV-2 infected K18-hACE2 mouse (6 dpi) immunostained with SARS-CoV-2 (N, green) and vascular (IB4; red) markers indicating the lack of significant SARS-CoV-2$^+$ staining associated with IB4$^+$ blood vessels. Nuclei were counterstained with DAPI (blue) in merge images (A-C).

A

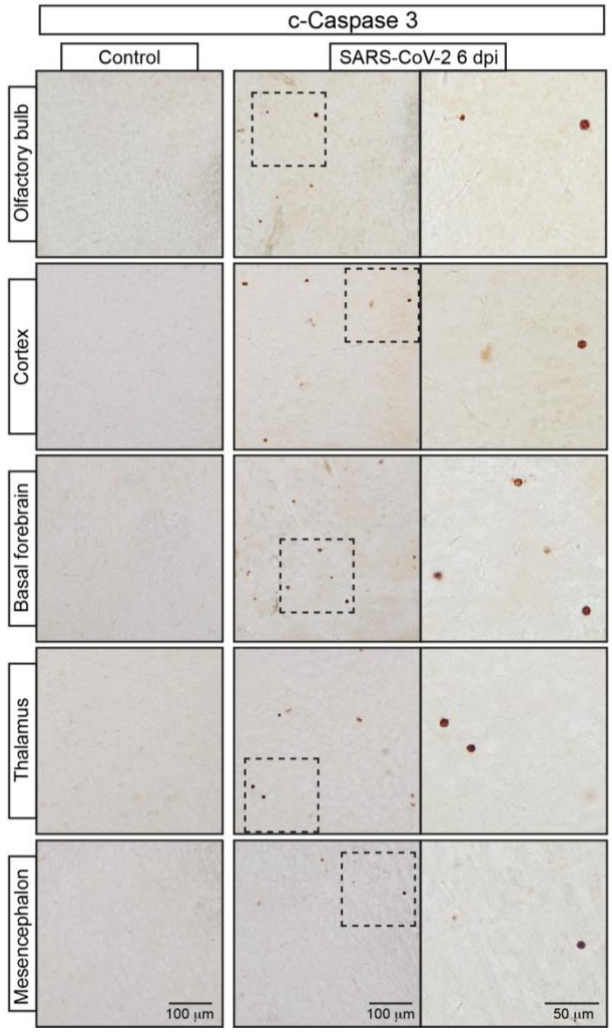

B

	c-Caspase 3	
	SARS-CoV-2	
	4 dpi	6 dpi
Olfactory bulb	ND	5/5
Cortex	0/3	3/5
Striatum	0/3	3/5
Basal forebrain	1/3	5/5
Hippocampus	1/3	4/5
Amygdala	1/3	4/5
Thalamus	1/3	5/5
Hypothalamus	1/3	5/5
Mesencephalon	1/3	4/5
Pons	1/3	4/5
Cerebellum	0/3	0/3

Supplementary Figure 3. SARS-CoV-2 cerebral infection produces cellular apoptosis. A. Light-transmitted images of the indicated cerebral regions from control and SARS-CoV-2 infected K18-hACE2 mice (6 dpi) after c-caspase-3 immunohistochemistry. Images in the right column depict, at higher magnification, the insets of the central column. B. Qualitative analysis of cellular apoptosis, induced by SARS-CoV-2 infection, in different cerebral regions. In brackets the number of mice showing c-casp3^{+} cells among the total number of mice studied is indicated for each brain region analyzed. ND, not determined.

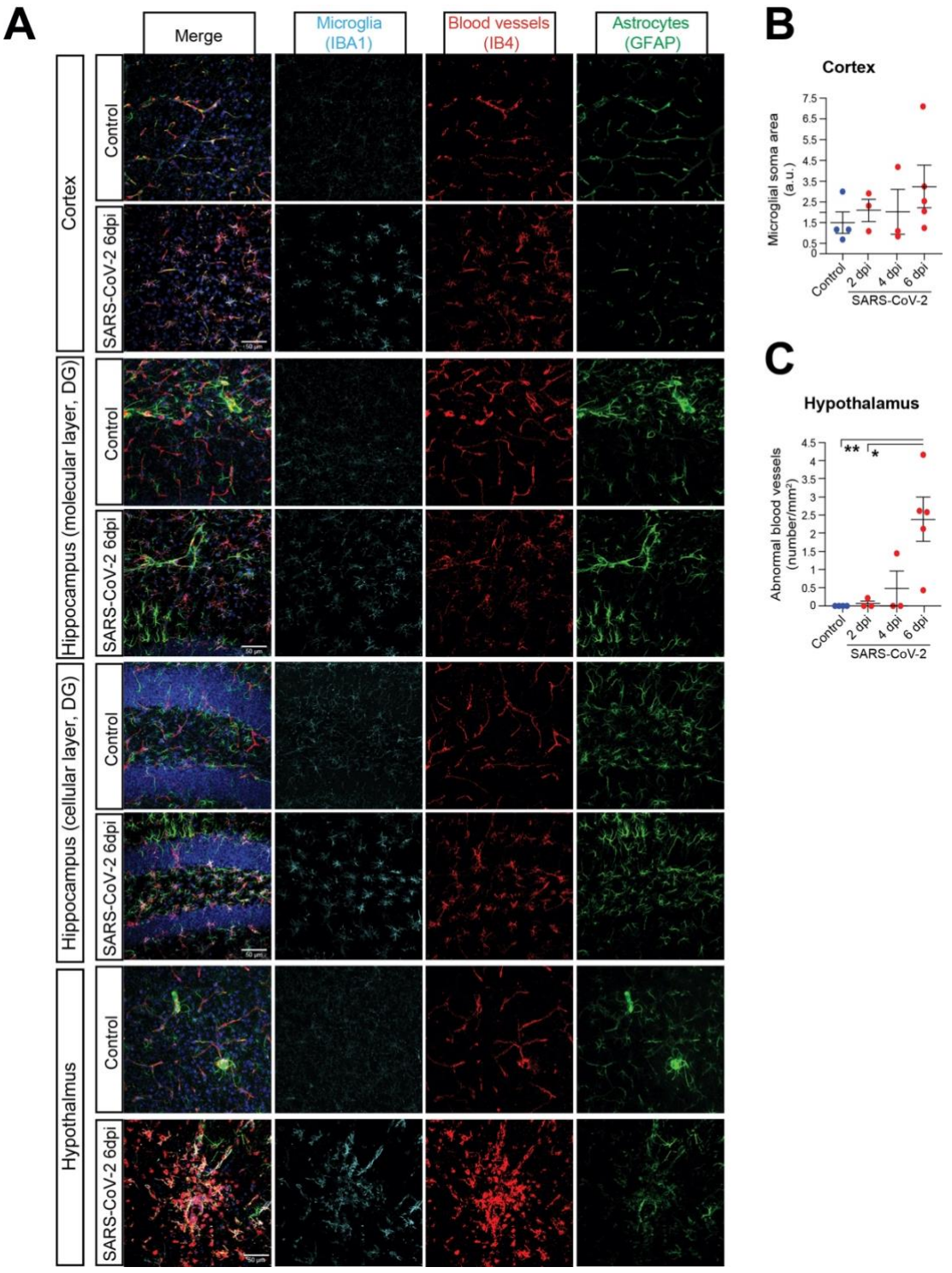

Supplementary Figure 4. Neuroinflammatory and vascular damage in SARS-CoV-2 infected brain. A. Confocal Z-projection images from control and SARS-CoV-2 infected K18 mice stained with microglial (IBA1; cyan), vascular (IB4; red), and astrocytic (GFAP, green) markers. B. Quantification of the microglial soma area in the cortex of control and SARS-CoV-2 infected mice. C. Analysis of the presence of abnormal blood vessels in the hypothalamus of the experimental groups indicated above. Nuclei were counterstained with DAPI (blue) in the merge images. Data are presented as mean ± SEM. Controls, n=4; SARS-CoV-2: 2 dpi, n=3; 4 dpi, n=3; and 6 dpi, n=5 mice. ANOVA, post hoc Tukey's test (B) or Kruskal-Wallis test; post hoc Dunn's test (C); *p<0.05; **p<0.01. DG: dentate gyrus.

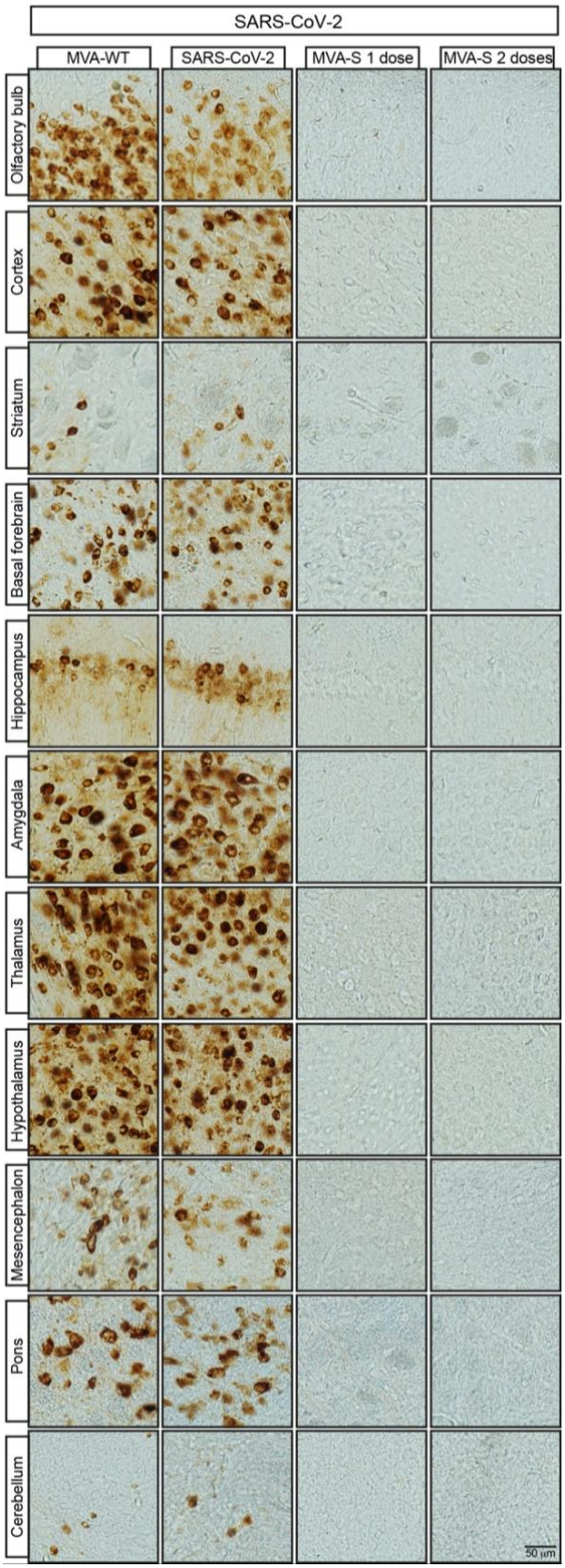

Supplementary Figure 5. MVA-CoV2-S vaccination prevents SARS-CoV-2 brain infection. Images of light-transmitted microscopy, after SARS-CoV-2 N immunohistochemistry, of the indicated cerebral regions showing the total protection conferred by the MVA-S vaccine (1 or 2 doses) against cerebral SARS-CoV-2 infection, in the reinfection experiment (6 dpi).